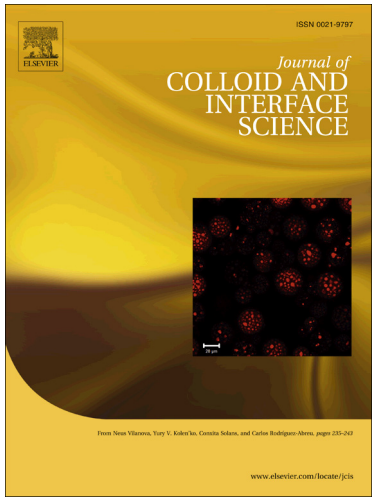

Carbon disulfide mediated self-assembly of Laccase and iron oxide nanoparticles on gold surfaces for biosensing applications

I. Almeida, F. Henriques, M.D. Carvalho, A.S. Viana

PII: S0021-9797(16)30697-X
DOI: http://dx.doi.org/10.1016/j.jcis.2016.09.042
Reference: YJCIS 21594

To appear in: *Journal of Colloid and Interface Science*

Received Date: 20 July 2016
Revised Date: 15 September 2016
Accepted Date: 16 September 2016

Please cite this article as: I. Almeida, F. Henriques, M.D. Carvalho, A.S. Viana, Carbon disulfide mediated self-assembly of Laccase and iron oxide nanoparticles on gold surfaces for biosensing applications, *Journal of Colloid and Interface Science* (2016), doi: http://dx.doi.org/10.1016/j.jcis.2016.09.042

Carbon disulfide mediated self-assembly of Laccase and iron oxide nanoparticles on gold surfaces for biosensing applications

I. Almeida, F. Henriques, M.D. Carvalho, A.S. Viana*

Centro de Química e Bioquímica. Faculdade de Ciências, Universidade de Lisboa, Edifício C8, Campo Grande, 1749-016 Lisboa, Portugal

*Corresponding Author: E-mail: anaviana@fc.ul.pt; Tel: +351217500864; Fax: +351217500088

Carbon disulfide mediated self-assembly of Laccase and iron oxide nanoparticles on gold surfaces for biosensing applications

I. Almeida, F. Henriques, M.D. Carvalho, A.S. Viana*

Centro de Química e Bioquímica, Faculdade de Ciências da Universidade de Lisboa, C8, Campo Grande, 1749-016 Lisboa, Portugal

Abstract

A simple one-step methodology was explored to prepare enzyme-modified nanostructured electrodes for the development of biosensing interfaces. Magnetite type nanoparticles conjugated with Laccase were immobilized on gold surfaces. This approach relies on the reaction between carbon disulfide and amine groups of biomolecules to form dithiocarbamate (DTC) moieties, as well as on the strong affinity between sulfur species and metals. Special emphasis was given to demonstrate DTC formation in aqueous solution and further attachment to iron oxide nanoparticles and to gold electrodes. UV-visible spectroscopy confirmed the functionalization of nanoparticles by DTC using a model secondary amine (N-hexylmethylamine). The direct attachment of modified iron oxide nanoparticles (with ca. 20 or 40 nm mean sizes) to gold electrodes was investigated using the hormone epinephrine, with well-known electrochemical properties. A high amount of immobilized epinephrine and a facilitated redox conversion was observed for modified electrodes containing iron oxide nanoparticles. The success of this simple and robust method was confirmed by X-ray photoelectronic spectroscopy. Finally, the catalytic activity of modified gold with iron oxide nanoparticles and Laccase was evaluated toward 2,2'-azino-bis (3-ethylbenzothiazoline-6-sulphonic acid diammonium salt (ABTS). Chronoamperometric studies revealed a significant catalytic activity of immobilized Laccase in the presence of the nanoparticles, in particular for the largest ones (40 nm), with a sensitivity for ABTS oxidation of 100 mA M^{-1} cm^{-2}.

Keywords: *in situ* dithiocarbamate formation; biomolecule immobilization; magnetic nanoparticles; enzyme-modified electrodes; electrochemical biosensor.

1. Introduction

Immobilization of enzymes on an appropriate support is a crucial step for the construction of biosensors and many efforts have been made in this field [1-3], especially combining enzymes with conductive materials [4-6]. The attachment of biomolecules on semiconducting metal oxide surfaces, such as magnetic iron oxide nanoparticles (Fe_3O_4 NPs), has been increasingly investigated, since these nanomaterials ensure the preservation of enzyme biological activity, with an amplification of the electrochemical signal [4-7]. This is due to the excellent biocompatibility, large specific surface area and good conductivity of nanoparticles at a nanoscale dimension that permits the wiring of redox-centers in proteins [8-11]. Well-established magnetic nanoparticles, such as Fe_3O_4 (magnetite) and γ-Fe_2O_3 (maghemite), are the most promising candidates for biosensing applications [12-14]. They can be easily prepared by the co-precipitation method in an acidic or alkaline solution, which will confer to the hydrophilic magnetite nanoparticles, a positive or a negative charge, respectively [15]. The solvents and coating agents are carefully chosen to prevent particle aggregation, forming nanoparticles with uniform sizes, and also to allow further surface functionalization [16-19]. The functionalization step is critical for the successful application of iron oxide nanostructures in biological fields [20]. In addition, an efficient immobilization of nanobioconjugates to an electrode surface is another challenging task to prepare biosensing interfaces with electrochemical transduction.

In situ formation of DTC groups, through the one-step reaction between carbon disulfide and an amine group, provides a stable and direct method to bind biomolecules to gold surfaces [21, 22]. This surface modification approach is an alternative to the widely used alkanethiols self-assembled monolayers on gold, which requires an activation step to promote the covalent attachment of biomolecules [23]. The interaction between sulfur species and metal oxides has been critically reviewed [24], highlighting

the qualitative relationship between the band gap energy of the metal oxides and their reactivity towards sulfur. Metal oxides with small band gaps (such as Fe_3O_4 (ca. 2.1 eV) [25] exhibit a good interaction with sulfur moieties, due to their ability to displace valence electrons [24]. The efficient linkage of thiols to iron oxide nanoparticles has been proved by capping the nanoparticles with cysteine [26]. Recently, we also demonstrated that carbon disulfide could be used to readily attach iron oxide nanoparticles to a gold electrode [27]. The catalytic surfaces of such electrodes were positively tested for oxygen reduction reaction.

There are many other reports addressing the successful immobilization of biologic compounds onto Fe_3O_4 nanoparticles *via* covalent linkages [7, 12, 28], layer-by-layer deposition [29] or through polymerization methods [13, 14]. Most of these reports used glucose oxidase, although there are also a few studies concerning the covalent immobilization of Laccase on magnetite nanoparticles. These works use mostly amine functionalized core-shell Fe_3O_4/SiO_2 nanoparticles [12] and glutaraldehyde [30-32] as crosslinking agent. In the majority of the reported approaches using Laccase the enzyme-linked nanoparticles were drop-casted on carbon electrodes and their biological activity tested electrochemically.

The enzyme Laccase is recognized for its technological applications, namely in the development of biosensors for the quantitative determination of phenols in food, environment and body fluids [13, 33]. This enzyme is polymeric and contains four copper atoms, distributed into 3 types of redox sites, named T1, T2, and T3, where T2 and T3 are close together forming a trinuclear copper cluster. Laccase is able to catalyze the oxidation of ortho- and paradiphenols, polyphenols, and also of some aromatic di-amines and inorganic ions, with the simultaneous reduction of oxygen to water [34].

Herewith, we propose to use unmodified Fe_3O_4 nanoparticles and one-pot approach to modify gold electrodes with catalytic assemblies of Laccase/Fe_3O_4 nanoparticles, based on sulfur chemistry. This innovative method is simpler than those usually reported for the preparation of enzyme-magnetite nanoconjugates [12, 13]. The procedure depends on i) the *in situ* formation of DTC (from the reaction between the enzyme amine groups and CS_2) [35], ii) their linkage to Fe_3O_4 nanoparticles, and iii) on the attachment of the modified nanoparticles to the electrode surface. This last step may be formed by DTC (or unreacted CS_2) that can bridge between both interfaces. Due to the spontaneity of this approach, the direct attachment of DTC ligands (without nanoparticles) to the flat

surface is also expected. A schematic picture of the proposed surface modification approach is shown in figure 1.

The bioactivity of the Laccase modified electrodes is tested for the catalytic oxidation of 2,2'-azino-bis(3-ethylbenzothiazoline-6-sulphonic acid diammonium salt (ABTS). This is one of the best substrate for Laccase [36,37] and is electroactive, allowing the direct monitoring of enzyme oxidized species on the electrode surface. We have investigated the catalytic performance of two iron oxide nanoparticles batches, with average diameter sizes of 20 and 40 nm, as it is known [27,38] that the size of magnetite nanoparticles is directly related to their oxidation degree and consequently, their electrical conductivity. Smaller molecules containing amine groups (N-hexylmethylamine (HMA) and epinephrine) are also studied in this work, as proof-of-concept of the proposed surface modification method.

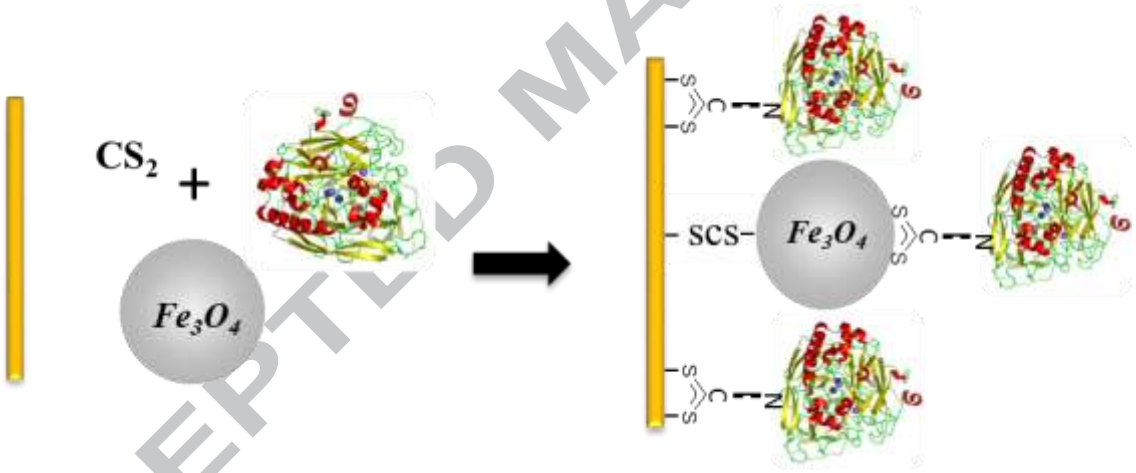

Figure 1 - Schematic representation of the one-step method exploited to modify gold surface with CS_2, Fe_3O_4 nanoparticles and Laccase.

2. Experimental

Chemicals

Carbon disulfide (Acros Organics), epinephrine (Sigma-Aldrich), HMA (Fluka), ABTS (Fluka), sulfuric acid (Pancreac), sodium hydroxide (Sigma-Aldrich), hydrogen

peroxide (VWR, Prolabo), phosphate buffer (8.0 mM Na_2PO_4 (Merck); 1.14 mM KH_2PO_4 (Merck); 138 mM NaCl (Merck) and 2.7 mM KCl (Merck); pH 7.0), citrate-phosphate buffer (0.1 M citric acid (Sigma-Aldrich), 0.2 M Na_2HPO_4 (Merck), pH 4.6) and absolute ethanol (Riedel-de Häen) were all analytical grade and used without further purification. Laccase *Trametes versicolor* (powder, 0.92 units/mg, Sigma-Aldrich) was also used without purification. Ultra-pure water was obtained from a MILLI-Q A10 Gradient purification system (resistivity of 18 MΩ cm at 25º C) and used to prepare all the solutions.

Synthesis of Fe_3O_4 nanoparticles

Fe_3O_4 NPs were synthetized according to the previously reported precipitation method [27, 38]. Stoichiometric amounts of $FeSO_4.7H_2O$ and $FeCl_3.6H_2O$ were dissolved in acidic medium under a nitrogen environment and NH_4OH was added to precipitate the Fe_3O_4 nanoparticles. The product was heated at 200ºC for 3 and 24 h (inside an autoclave) to obtain nanoparticles with approximately 20 and 40 nm average size, respectively. Magnetic filtration was employed to separate the magnetite nanoparticles, that were washed (with water until a neutral pH was obtained) and subsequently dried at 60ºC.

Characterization and functionalization of Fe_3O_4 nanoparticles

The particles size distribution was determined from transmission electron microscopy (TEM, Hitachi H-8100 operating at 10–15 kV) images, with the program ImageJ, measuring the size of ca. 80-100 nanoparticles for each sample. The morphology and average diameters of Fe_3O_4 NPs colloidal suspensions were characterized by Atomic Force Microscope (room temperature), by placing a drop of the colloidal suspension onto freshly cleaved mica for 15 min and let the solvent to dry out.

The functionalization of Fe_3O_4 NPs in colloidal suspension with HMA and CS_2 was investigated by UV–vis spectroscopy (UV-2600 spectrophotometer, Shimadzu). Fe_3O_4 NPs aqueous suspension was prepared through the addition of 3 mg of Fe_3O_4 NPs powder to 500 µL phosphate buffer solution (pH 7.0) following 15 min in ultra-sonic bath. 250 µL of the sonicated aqueous Fe_3O_4 NPs (20 or 40 nm) suspension were mixed with 3.75 µL CS_2 (0.25 mM) and 15 µL HMA (0.50 mM), during 2 hours. This reaction time was chosen to ensure dithiocarbamate absorption bands to be clearly detected [21].

After, using a magnet, the suspensions were rinsed five times with Millipore water, in order to guarantee that only the species strongly bonded to the nanoparticles were maintained, while the remaining compounds were removed in the washing process. It is known that DTC formation is promoted in basic solutions [40] but still occurs quantitatively at neutral pH [22, 35, 39]. The reaction was conducted at pH 7.0 as a compromise between enzyme stability and DTC reaction conditions.

Gold Electrodes

A gold film (200 nm) deposited on borosilicate glass (pre-layer of chromium, 2 – 4 nm) from Arrandee^{TM} was used as working electrode. The surface was cleaned with piranha solution (3:1 mixture (v/v) of H_2SO_4:H_2O_2), rinsed with ultrapure water and ethanol, and flame annealed, leading to a predominant (111) crystallographic orientation and a surface roughness of 1.2. The morphological characterization of bare gold surfaces has been previously described [21].

Gold surface modification

Au surfaces were modified by immersion in Fe_3O_4 NPs aqueous suspension (3 mg of Fe_3O_4 NPs powder in 500 µL phosphate buffer solution (pH 7.0), prepared as described above) mixed with i) CS_2 (0.1 M), ii) CS_2 (0.1 M) and epinephrine (0.1 M) at room temperature, or iii) CS_2 (0.1 M) and Laccase (1 mg/mL) at 4 °C, during 16 h

Atomic Force Microscopic characterization

The morphology of modified Au electrodes with CS_2 and Laccase with or without Fe_3O_4 NPs (20 and 40 nm) were characterized by *tapping* mode AFM, using a Nanoscope IIIa Multimode (Digital Instruments, Veeco). Etched silicon tips (~300 KHz) and a scan rate of ca. 1.6 Hz were used for imaging.

Electrochemical measurements

A three electrode Teflon cell was employed to perform the electrochemical experiments with gold slide as working electrode. A saturated calomel electrode (SCE) and a platinum foil served as the reference electrode and the counter-electrode, respectively.

The geometric area of working electrode (0.57 cm^2) was defined by an *o-ring*. Electrochemical assays were performed using a PARSTAT 2263 electrochemical work station produced by PerkinElmer. The electrolyte solutions were degassed with nitrogen (99.99997%) prior to each experiment for 15 min, except for the electrochemical reductive desorption assay, that required longer degassing periods (60 min) to ensure the total removal of oxygen (in the potential range used for the experiments any residual oxygen will originate a reduction peak that would mask the sulfur desorption process). Single-step chronoamperograms were recorded by stepping the potential from open circuit potential to 0.41 V *(vs. SCE)*.

XPS characterization

X-ray photoelectron spectroscopy (XPS) was performed at Centro de Materiais da Universidade do Porto (CEMUP, Portugal), using a Kratos AXIS Ultra HSA with VISION software for data acquisition. The spectra were acquired with a monochromatic Al Kα X-ray source (1486.6 eV), operating at 15 kV (90 W), in the fixed analyzer transmission mode (FATmode), with a pass energy of 40 eV for regions ROI and 80 eV for survey. Data acquisition was performed at a pressure lower than $1x10^{-6}$ Pa, and it was used as a charge neutralization system. The effect of the electric charge was corrected with reference to the C1s peak (285 eV). The spectra were deconvoluted with the XPSpeak software, using a Gaussian–Lorentzian peak shape and Shirley (or Linear) type background subtraction.

3. Results and Discussion

3.1 *In situ* formation of dithiocarbamates/Fe_3O_4 NPs assemblies in colloidal suspension

TEM and AFM images of the Fe_3O_4 NPs used throughout this work, as well as the corresponding histograms and topographic profiles are shown in figure S1

(Supplementary Material). The size distribution histograms obtained by TEM images exhibit average diameters of 20 ± 5 nm and 41 ± 9 nm, for the two batches of nanoparticles used, as expected under the synthetic conditions used [27], and perfectly match the corresponding cross-sections on AFM images. The values of 20 nm and 40 nm will be used to identify each nanoparticle sample. XRD patterns of these type of Fe_3O_4 nanoparticles [27], 40 nm sample exhibits a cell parameter (a = 8.394(3) Å) close to bulk magnetite, corresponding to less oxidized nanoparticles than the 20 nm nanoparticles (a = 8.386(5) Å), due to the lower surface area/volume ratio.

A secondary amine, HMA was chosen to react with CS_2 and Fe_3O_4 NPs (20 and 40 nm) to confirm the functionalization of nanoparticles in aqueous suspension *via* the formation of *in situ* DTC groups. The UV-visible characterization of the aqueous and colloidal suspensions of CS_2, HMA, Fe_3O_4 NPs (40 nm) and CS_2/Fe_3O_4 NPs/HMA is shown in figure 2. The colloidal suspension of Fe_3O_4 nanoparticles (40 nm) absorb in the studied wavelength window. HMA displays two absorption bands, one more intense at 250 and a small shoulder at 288 nm (figure 2). CS_2 molecules exhibit a peak near 315 nm within the investigated wavelengths which intensity is known to decrease remarkably over time in the presence of amine groups [39]. After the reaction with CS_2 and HMA, the modified nanoparticles were extensively washed using a magnet, and re-suspended in buffer solution. The presence of typical bands of DTC can be confirmed by the UV–vis spectrum (thick red line in figure 2) through the presence of two absorption bands at 255 nm and 281 nm similarly to the reported values for DTC (260 and 290 nm) [22, 40]. Similar studies were performed with 20 nm Fe_3O_4 NPs (figure S2, Supplementary Material). Spectrophotometric data confirm the one-step formation of dithiocarbamate on Fe_3O_4 NPs (20 and 40 nm), and the suitability of this approach for a straightforward functionalization of unmodified magnetite nanoparticles.

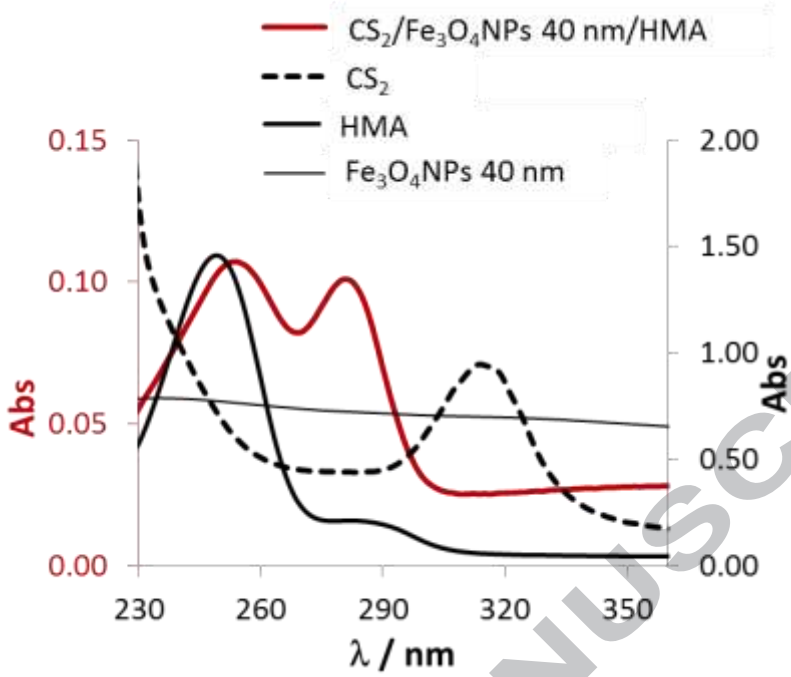

Figure 2 - UV–vis spectra of the CS_2, HMA, Fe_3O_4 NPs (40 nm) and CS_2/Fe_3O_4 NPs (40 nm) /HMA, in phosphate buffer solution (concentrations are 0.25 mM and 0.50 mM for CS_2 and HMA, respectively).

3.2 *In situ* formation of dithiocarbamates/Fe_3O_4 NPs assemblies on gold surfaces

3.2.1 Modified electrodes with epinephrine

Cyclic voltammetry was used to investigate the functionalization of gold electrodes with Fe_3O_4 NPs modified with amine compounds. To achieve this goal, the electrodes have been exposed to aqueous solutions of CS_2, Fe_3O_4 NPs and epinephrine (an electroactive, secondary amine [21]) following the one-pot approach illustrated in figure 1. The electrochemical characterization of the modified electrodes was performed in 0.1 M H_2SO_4 (pH 1.1) since this is an appropriate acidic solution to study the epinephrine redox behavior [21]. In order to prove the immobilization of Fe_3O_4 NPs by CS_2, the electrochemical response of these modified electrodes was firstly investigated (figure 3a). A cyclic voltammogram corresponding to the gold electrode upon immersion in only CS_2 (absence of nanoparticles), recorded in the same conditions, is also provided for comparison. A redox process (E_p^{ox} = 0.53 V and E_p^{red} = 0.41 V) can be

depicted in the voltammogram of the modified electrode with CS_2 and Fe_3O_4 NPs, which was shown to be stable within potential cycling in acidic medium (10^{th} cycle is also included in figure 3a). The linear dependence of the anodic peak currents with the sweep rate is shown in the inset of figure 3a, indicating a charge-controlled electron transfer process, as expected for immobilized electroactive species (the slope obtained from the representation of log j_p^{ox} *vs.* log υ is 0.84, which is close to the ideal value of 1.0 predicted for pure surface-confined species electronic transfer [41,42]). The process is assigned to the electrochemical conversion of Fe^{II} /Fe^{III} in Fe_3O_4 NPs, not yet well documented for magnetite nanoparticles, but consistent with the potential values recorded for bulk Fe_3O_4 [43]. A similar electrochemical behavior of this modified surface (Au/CS_2/Fe_3O_4 NPs 40 nm) has been also observed in different pH solutions (figure S3 Supplementary Material), proving the stability of the interfaces. pH 7.0 was chosen since it is adequate to carry out a number of enzyme catalytic studies, whereas pH 4.6 is the optimal pH to study Laccase catalytic activity [37]. At pH 7 the oxidation/reduction processes occur at slightly less positive potential values (0.47 and 0.39 V) than at pH 4.6 (0.53 and 0.41 V), as shown in figure S3a and b (Supplementary Material), respectively.

As demonstrated by the results presented above, modified electrodes with iron oxide nanoparticles and CS_2 are stable during the electrochemical experiments in acidic medium. This fact is attributed to the spontaneous formation of a CS_2 protective organic coating on the surface of the nanoparticles, together with the formation of a robust link to the gold surface. This is a relevant finding since it turns viable the use of unmodified iron oxide nanoparticles to functionalize electrode surfaces.

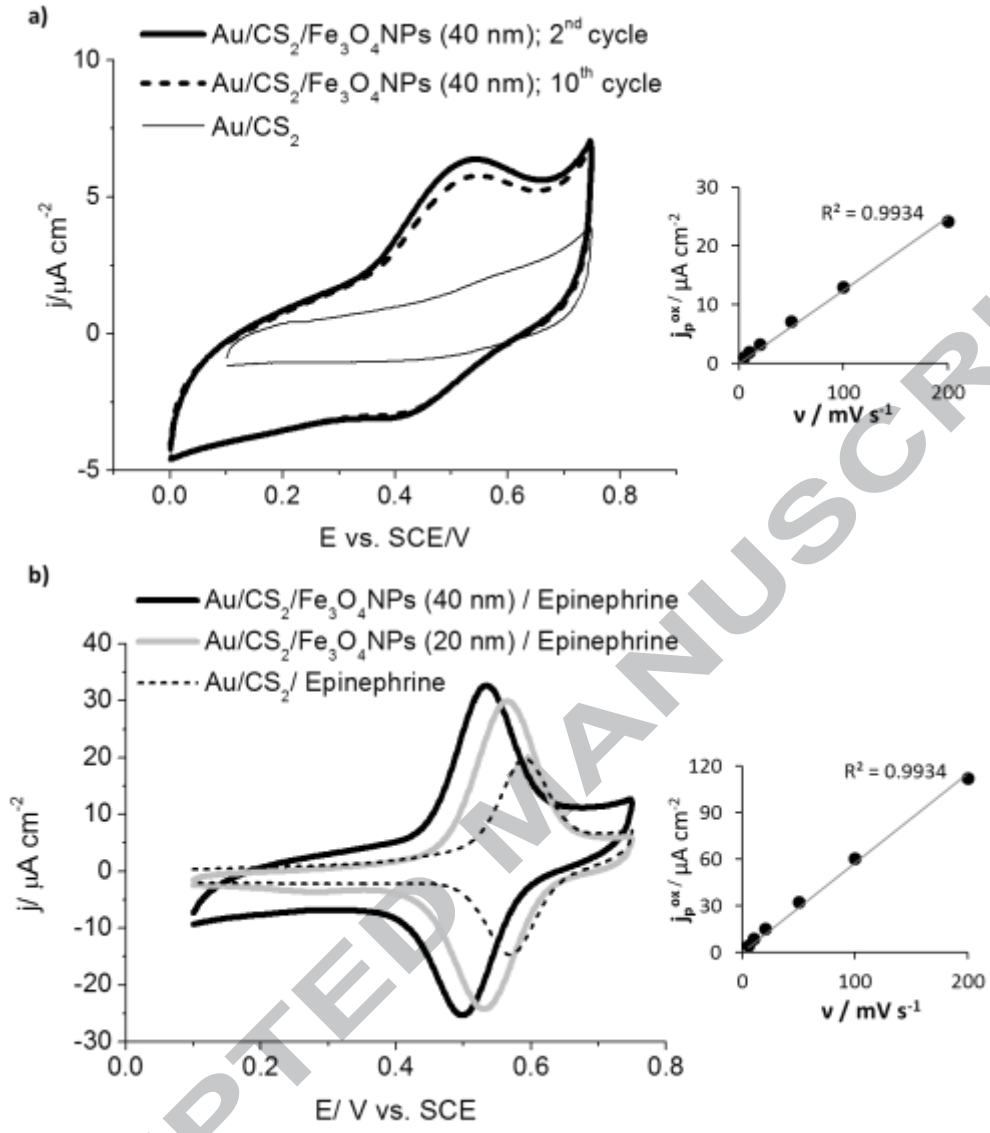

Figure 3– Cyclic voltammograms (2nd and 10th cycles) of modified gold electrodes with CS_2/Fe_3O_4 NPs (40 nm), in 0.1 M H_2SO_4 at 50 mV s^{-1}; b) CS_2/Epinephrine in the presence and absence of Fe_3O_4 NPs in 0.1 M H_2SO_4 and ν = 50 mV s^{-1}; Inset of figures: j_p^{ox} *vs.* υ.

The redox studies of modified surfaces in the presence of epinephrine with or without Fe_3O_4 NPs (20 and 40 nm) are shown in figure 3b. It is verified that in the presence of nanoparticles, the oxidation and reduction peaks attributed to the hydroquinone/quinone forms of epinephrine [21, 35] are nearly symmetric, with half-wave potentials negatively shifted regarding the one observed for modified gold in the absence of Fe_3O_4 NPs ($E_{1/2}$ = 0.58 V). Values of $E_{1/2}$ = 0.55 and 0.51 V were obtained for Fe_3O_4 NPs with 20 and 40 nm, respectively, indicating a slightly facilitated electron

transfer process of epinephrine linked to the larger nanoparticles, which is consistent to a less oxidized magnetite surface for the 40 nm nanoparticles, as previously referred. The linear behavior between j_p and υ (inset of figure 3b) supports the stable surface-confinement of epinephrine [35].

The cyclic voltammograms recorded at 50 mVs^{-1} (figure 3b) for the modified electrodes with magnetite nanoparticles and epinephrine do not allow distinguishing between the redox processes of Fe_3O_4 NPs and catecholamine. However, at a low sweep rate (5 $mV\ s^{-1}$) these processes can be clearly depicted at both pH 1.1 and 7.0, as can be observed from figure 4. It is noteworthy that while the potential values of the redox peaks assigned to Fe_3O_4 NPs do not change significantly (redox peaks I), the epinephrine conversion (redox process II) shifts dramatically with pH, as expected for a $2e^-$ and $2H^+$ electron transfer process [21, 27]. These results corroborate the assignment of both electrochemical processes and prove the presence of the two adsorbates (Fe_3O_4 NPs and epinephrine) on the electrode surface.

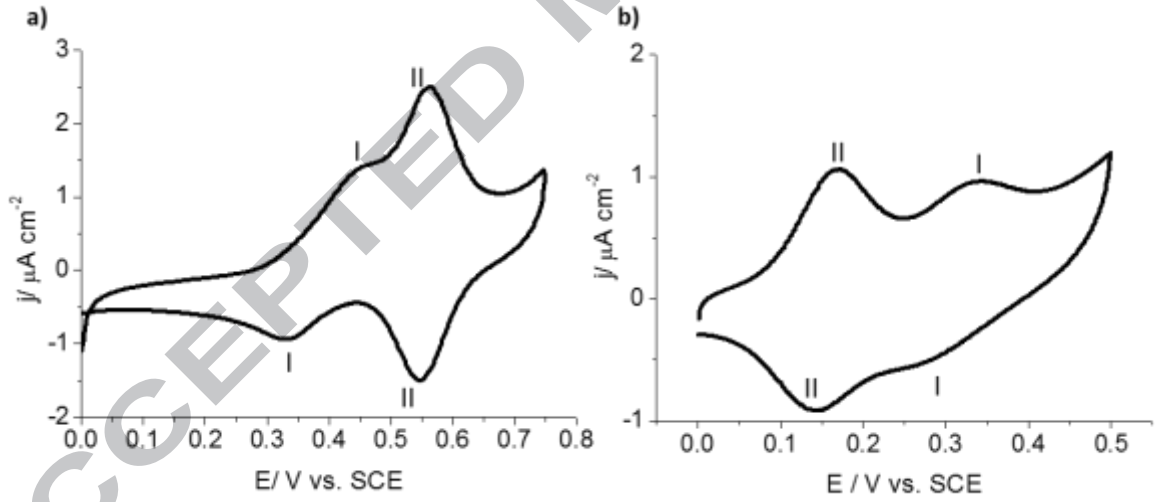

Figure 4 – Cyclic voltammograms of modified electrodes with CS_2, epinephrine, Fe_3O_4 NPs (20 nm) in: a) 0.1 M H_2SO_4 and b) phosphate buffer solution (pH 7.0), at 5 mVs^{-1}.

Epinephrine surface coverages were estimated based on the integration of the oxidation processes (figure 3b), considering the transfer of two electrons. The addition of Fe_3O_4 NPs into the surface reaction resulted in a great increase of epinephrine surface concentration from 1.5×10^{-10} (without Fe_3O_4 NPs) to 2.5×10^{-10} (Fe_3O_4 NPs with 20 nm) and 2.7×10^{-10} (Fe_3O_4 NPs with 40 nm) mol cm^{-2}, proving the efficiency of this novel one-pot reaction to immobilize epinephrine, and thus amine compounds, in an

aqueous environment. It is worth to note that epinephrine surface coverages of modified electrodes with nanoparticles can be slightly lower, as part of the charge (ca. 20 % based on the result of figure 3a) could be assigned to the Fe_3O_4 NPs redox conversion.

In order to confirm that Fe_3O_4 NPs were attached to the gold surface by sulfur moieties, a reductive desorption of the modified electrode with CS_2 and Fe_3O_4 NPs in alkaline medium has been performed and is illustrated in figure S4 (Supplementary Material). The two reduction peaks observed at -0.92 V and -0.76 V may be associated to different sulfur environments: Au – S_2C [35] and Au-S-C-S-Fe_3O_4 NPs. According to Cohen et al. [26], the adsorption of sulfur to iron oxide nanoparticles should occur mainly through a strong Fe-S chemical bond.

XPS analysis was performed on CS_2/Fe_3O_4 NPs/epinephrine modified electrode aiming to characterize the surface bonds established during the one-step modification. The S2p spectrum (figure 5) shows two main peaks fitted to the typical doublet ($S2p_{3/2}$ and $S2p_{1/2}$), where the binding energy position of the $S2p_{3/2}$ signal is taken as reference for the $S2p_{3/2\text{-}1/2}$ spin-orbit pair (Δ=1.2 eV) with a corresponding ratio of 2:1 [44]. $S2p_{3/2}$ and $S2p_{1/2}$ components have binding energies of 161.9 eV and 163.1 eV, respectively, and are assigned to the chemisorption of in situ generated DTC and carbon disulfide on the gold surface [35]. These binding energies are typical of ionic or covalently bound dithiocarbamates [45] or thiols on flat gold surfaces [46] and of thiols chemically bound to Au nanoparticles (3D assemblies) [44, 47]. Besides, as S-Fe bonds are expected to have similar binding energies for S2p3/2 [48], the observed peaks may also have the contribution of the sulfur-iron oxide nanoparticles linkages formed in the one-step methodology used. It is worth noting that no oxidized sulfur species (S2p > 166 eV [49]) were observed in this work, supporting the most probable formation of Fe-S bond.

A much less intense $S2p_{3/2,1/2}$ doublet occurs at 163.8 and 164.7 eV binding energies, values usually attributed to physisorbed or unbonded thiols or thiolates or to the formation of disulfides [46,50], indicating that a small fraction of sulfur species is probably not chemically attached to metal surfaces.

The N1s peak of modified surfaces are detected at 399.8 eV, which is the value expected for N-C linkage in DTC, unequivocally demonstrating the formation of these groups by using CS_2 and epinephrine in the presence of Fe_3O_4 NPs [45, 51].

The Fe2p spectra was very diffuse (not shown) not allowing to use it for further investigation of Fe-S bonds. This fact is acceptable due to the low number of NP on the surface when compared to the casting procedures usually employed for XPS studies [52,53].

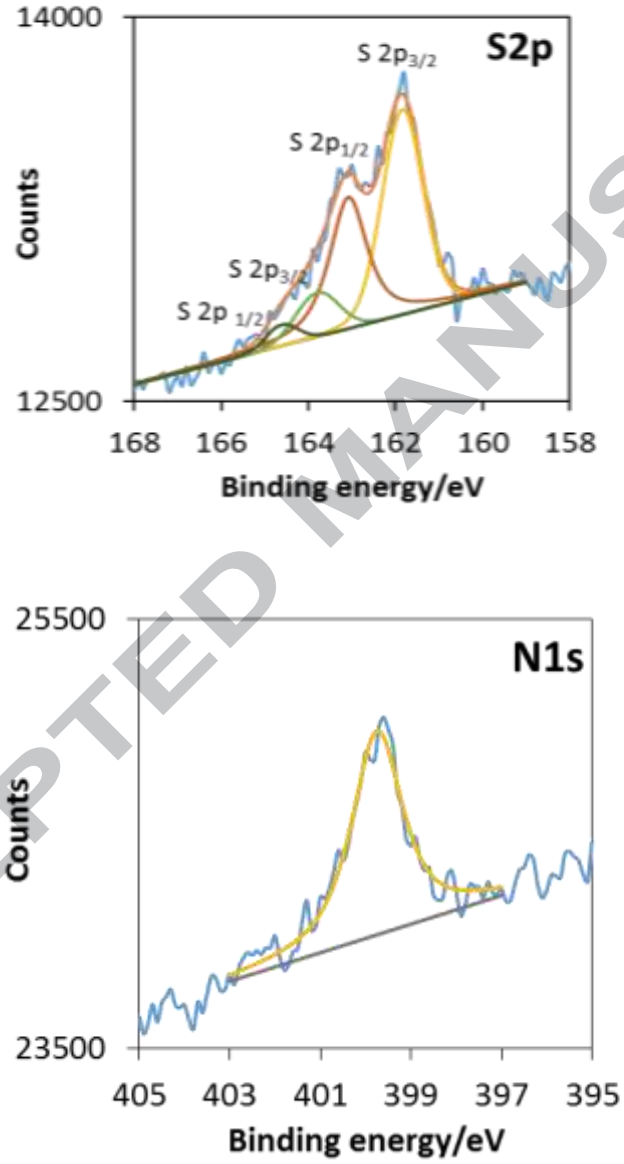

Figure 5 - XPS S2p, N1s, binding energies spectra of modified electrode with CS_2/Fe_3O_4NPs/epinephrine.

3.2.2 Modified electrodes with Laccase

The main purpose of this work, as mentioned before, is to use the reaction between CS_2, Fe_3O_4 nanoparticles and amine groups to immobilize enzymes on gold surfaces. To ascertain this possibility, we have studied the recognized catalytic activity of Laccase for ABTS [36], and expect that the combination with magnetite nanoparticles will enhance the catalytic activity of Laccase.

A morphological analysis of modified gold electrodes was carried out by atomic force microscopy. From figure 6a, showing AFM images of the electrode modified with CS_2 and Fe_3O_4 NPs, it is possible to depict both individual and agglomerated nanoparticles attached to the gold surface. The spontaneity of this surface modification method and the excess of CS_2 in solution allows CS_2 molecules to link individual nanoparticles to the substrate, as well as to establish bonds between nanoparticles (each sulfur binding one nanoparticle), building up some aggregates that can be also attached to the gold surface.

The AFM image of the modified electrode with CS_2/Fe_3O_4 NPs (40 nm)/Laccase, shown in figure 6b, reveals a fully covered surface with dispersed nanostructures with two distinct size population. One with ca. 40 to 80 nm, consistent with the functionalized Fe_3O_4 NPs assemblies adsorbed on the electrode, and the other, with smaller dimensions, up to ca. 20 nm, attributed to individual Laccase molecules linked by CS_2, as proposed in the schematic representation of figure 1. For comparison, a typical AFM image of modified electrodes only with Laccase and CS_2 is also depicted in figure 7c. In this case, the electrode surface is covered with small globular features (ca. 14 to 20 nm), consistent to adsorbed Laccase molecules by CS_2 (taking into consideration the tip convolution effects in AFM imaging that slightly enlarge the diameter of enzyme) [54]. These observations support the identification of the two distinct assemblies in figure 6b.

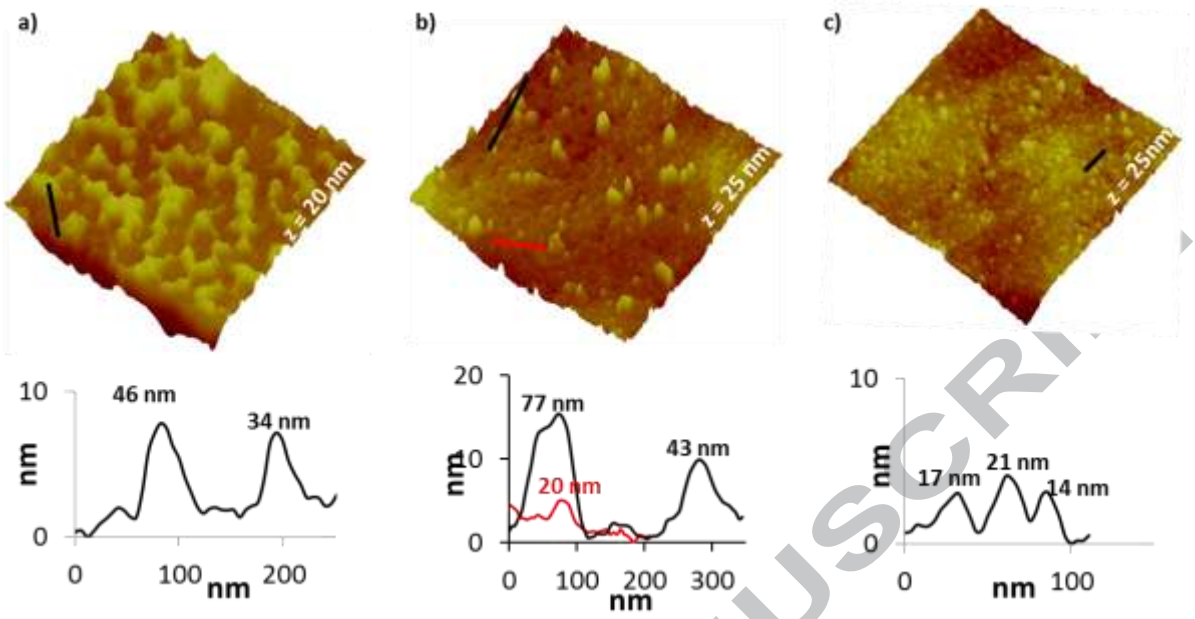

Figure 6 - AFM images (1.0 × 1.0 μm^2) and corresponding profiles of modified Au electrode with a) CS_2/Fe_3O_4 NPs (40 nm), b) CS_2/Fe_3O_4 NPs (40 nm)/Laccase and c) CS_2/Laccase.

The enzymatic activity of Laccase immobilized by CS_2, towards the oxidation of ABTS, was investigated in the presence and absence of Fe_3O_4 NPs (20 and 40 nm) in citrate-phosphate buffer solution (pH 4.6). According to the equations 1 and 2, described below [55], Laccase oxidizes ABTS and recovers the oxidized form through the reduction of O_2 to H_2O. The oxidized ABTS is then reduced at the electrode surface (eq. 3, direct reaction pathway), which is the electrochemical reaction that is followed by cyclic voltammetry or chronoamperometry. A sigmoidal-shape catalytic cyclic voltammogram is expected in presence of ABTS and O_2, when the enzyme is biologically active [33]. In contrast, the redox conversion of 0.5 mM ABTS on bare gold electrode (absence of enzyme) has a reversible behavior (in agreement with eq. 3) and occurs at $E_{1/2}$ = 0.46 V (ΔE_p = 0.12 V at pH 4.6), as shown in figure S5 (Supplementary Material).

$$Lacc4Cu^{(II)} + 4ABTS^{2-} \leftrightarrow 4ABTS^{\cdot-} + Lacc4Cu^{(I)} \quad \text{(eq. 1)}$$

$$Lacc4Cu^{(I)} + O_2 + 4H^+ \rightarrow 2\,H_2O + Lacc4Cu^{(II)} \quad \text{(eq. 2)}$$

$$4ABTS^{\cdot-} + 4e^- \leftrightarrow 4ABTS^{2-} \quad \text{(eq. 3)}$$

Figure 7a shows the electrochemical behavior of Fe_3O_4 NPs attached to the gold surface by CS_2 (in the absence of Laccase) in 10 µM ABTS. Both oxidation and reduction processes of ABTS are clearly depicted, in contrast to the absence of any redox signals obtained for a gold electrode only modified with CS_2 (for this low ABTS concentration). The different behavior is probably due to the larger surface area, when the nanoparticles are present, and also to the positive role of Fe_3O_4 NPs in facilitating electron transfer between the electrode and the ABTS. In addition, the modified electrode prepared only with Fe_3O_4 NPs and Laccase (absence of CS_2 linker), does not show any electrochemical process assigned to ABTS, as shown in figure S6 (Supplementary Material). This result unequivocally proves the essential role of CS_2 in the immobilization process of iron oxide nanoparticles and bioactive Laccase.

For modified gold with only CS_2 and Laccase (figure 7b), small catalytic currents for ABTS reduction are depicted (no oxidation peaks are visible), which are considerably enhanced when Fe_3O_4 nanoparticles are added to the one-pot reaction, as observed in the case of CS_2/Fe_3O_4 NPs (40 nm)/ Laccase, in figure 7c. The shape of the cyclic voltammograms obtained for this modified electrode is sigmoidal-like, as expected for these catalytic reactions [55,56,]. The reduction currents are greatly enhanced regarding the corresponding oxidation ones as ABTS concentration increases (taking as reference the cyclic voltammogram obtained at 0 µM ABTS), due to the chemical oxidation of ABTS by the enzyme (eq.1). These voltammetric studies demonstrate that Fe_3O_4 nanoparticles improve the catalytic performance of these modified electrodes, similarly to that observed in the detection of hydroquinone [13], using a modified surface of Fe_3O_4 NPs/Polydopamine-Laccase/Au.

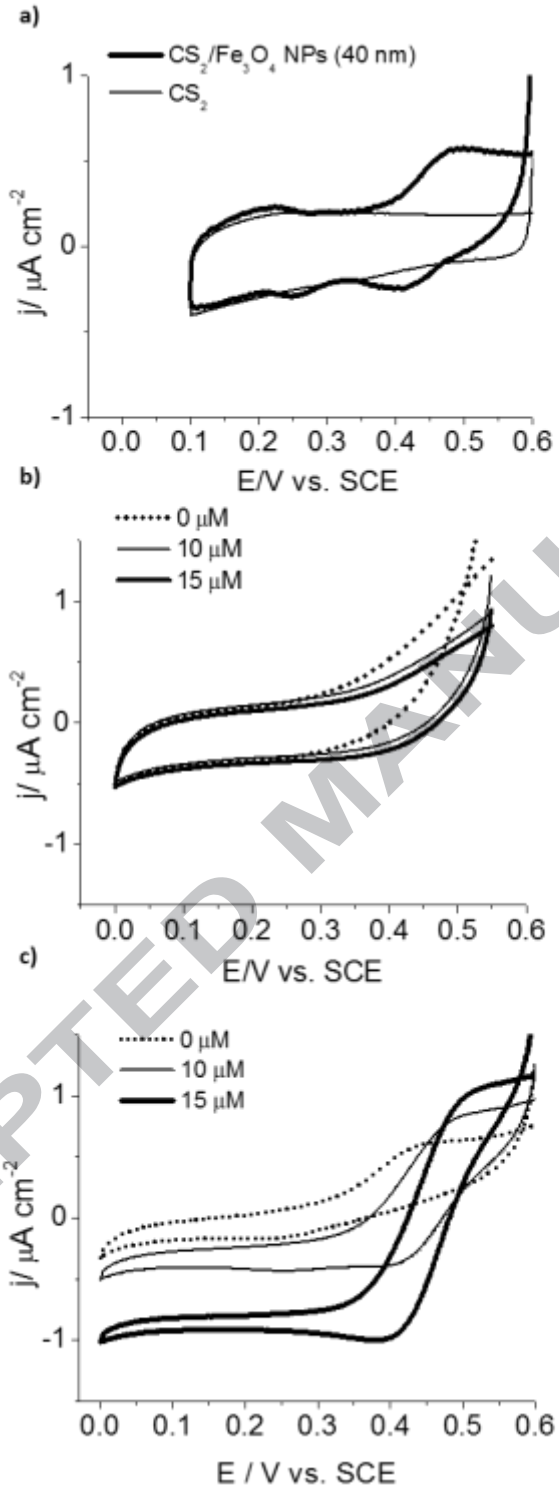

Figure 7– Cyclic voltammograms recorded at 5 mV s^{-1} in citrate-phosphate solution (pH 4.6) of modified electrodes with a) CS_2 or CS_2/Fe_3O_4 NPs (40 nm), in the presence of 10 µM of ABTS; b) CS_2/Laccase and c) CS_2/Fe_3O_4 NPs (40 nm)/Laccase in different concentrations of ABTS.

For a more accurate determination of the enzyme catalytic reaction sensitivity towards ABTS, chronoamperograms of the modified gold electrodes were recorded at 0.41 V (a value chosen from the cyclic voltammogram of ABTS shown in figure S5, Supplementary Material). The raw data and the $j-j_i$ *vs.* t representation (inset of figure) for CS_2/Fe_3O_4 NPs (40 nm)/Laccase electrode are shown in figure 8a (j_i corresponds to the current response of the modified electrode in the absence of ABTS, upon stabilization at 0.41 V). The results obtained for modified surfaces with CS_2/Fe_3O_4NPs (20 nm) /Laccase and CS_2/Laccase are presented in figure S7a and b, respectively (Supplementary Material). It is noteworthy that there is a clear decrease of the reduction currents ($j-j_i$) with increasing ABTS concentration, consistent with the catalytic process of Laccase towards ABTS, for the three enzyme-modified electrodes studied. In addition, the data exhibited in figure 8b, undoubtedly reveals that gold surfaces modified only with enzyme and CS_2, without nanoparticles, exhibited the lowest sensitivity (11 mA $M^{-1}cm^{-2}$), with the saturation of the enzyme at about 11 μM for the detection of ABTS. The best catalytic response was obtained for the enzyme linked to Fe_3O_4 NPs (40 nm) (figure 8b), with a sensitivity of 100 mA M^{-1} cm^{-2}; a value of about 70 % higher than that observed for CS_2/Fe_3O_4 NPs 20 nm/Laccase (28 mA M^{-1} cm^{-2}) and a wider linear range (up to 15 μM). The sensitivity value obtained for the modified electrode with 40 nm Fe_3O_4 NPs is higher than that determined in other studies for modified platinum or graphite surfaces with Laccase (from 35 to 75 mA M^{-1} cm^{-2}) for ABTS detection [33,57]. The best performance exhibited by the electrodes with the larger Fe_3O_4 NPs is consistent with the data obtained in electrocatalytic studies towards oxygen reduction reaction [27], carried out using similar iron oxide nanoparticles.

As previously stated [38], the general accepted formula of magnetite nanoparticles is $Fe_{3-x}O_4$, and the size of the iron oxide nanoparticles influences the degree of surface oxidation, i.e., *x* increases with NP size and consequently the amount of Fe^{2+} decreases. These phenomena imply that the structure of small nanoparticles has a large number of iron vacancies and less Fe^{2+}, hampering the electron hopping between Fe^{3+} and Fe^{2+}, and affecting their conductivity. Therefore, the good conductivity of the larger and less oxidized NP surface should contribute to the better catalytic activity of the enzyme-modified electrode with these nanoparticles. In addition, the amount of active enzyme on the modified electrodes must also contribute to the enhancement of the ABTS reduction currents.

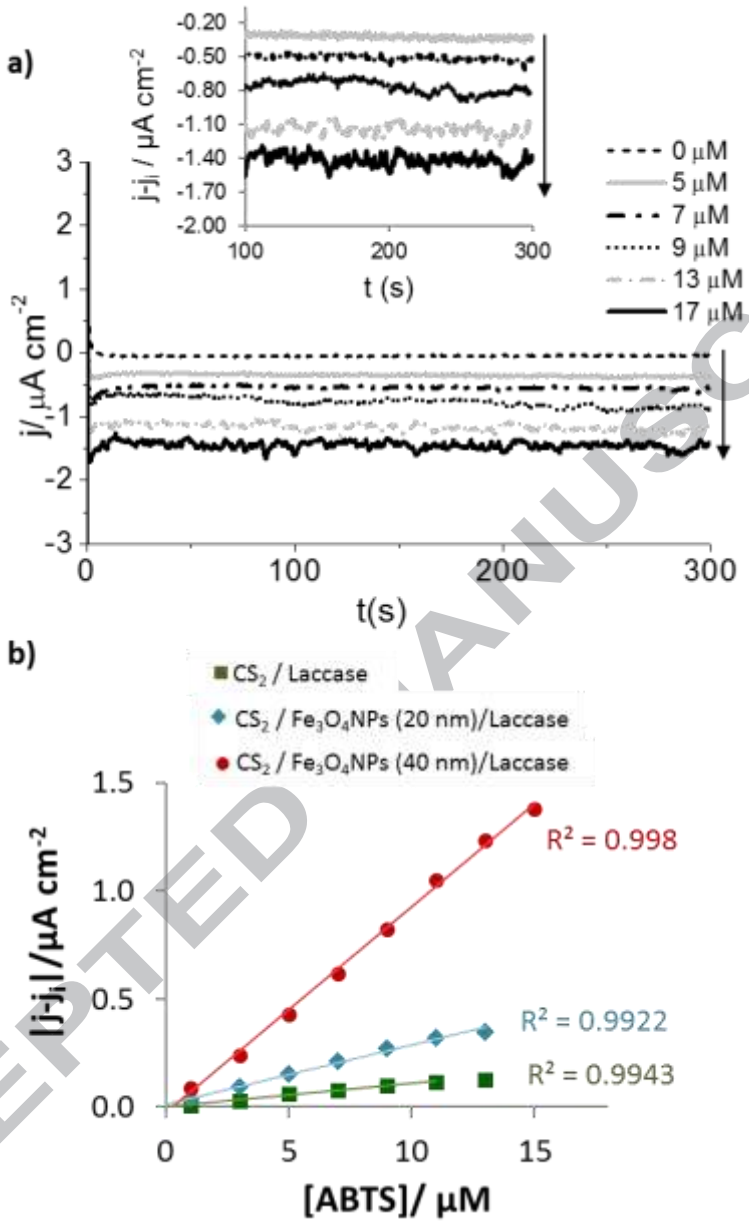

Figure 8 – a) Chronoamperograms of CS_2/Fe_3O_4 NPs (40 nm)/Laccase electrode obtained for increasing concentrations of ABTS at 0.41 V, inset: $j-j_i$ *vs.* t; b) representation of $|j-j_i|$ *vs* [ABTS] collected from chronoamperograms obtained for modified electrodes with CS_2/Laccase, CS_2/Fe_3O_4 NPs (20 nm)/Laccase and CS_2/Fe_3O_4 NPs (40 nm)/Laccase. All measurements were carried out in citrate-phosphate solution pH 4.6.

The direct electrochemical response of enzyme on the modified electrode CS_2/Fe_3O_4 NPs (40 nm)/Laccase was also studied by cyclic voltammetry, in deaerated citrate-phosphate buffer solution (pH 4.6), as shown in figure 9. At higher sweep rates, it is possible to observe two defined redox peaks. The first one, with $E_{1/2}$ = 0.26 V (ΔE_p = 0.06 V at 100 mVs^{-1}), is similar to that previously reported [58] for direct electron transfer of Laccase Cu^{II}/Cu^{I} at similar pH value, using the same Laccase fungal source (*Trametes versicolor*). Laccase from *Trametes versicolor* is classified as a high-potential enzyme, with type 1 Cu formal potential at ~ 0.78 V vs. NHE [59]. However, it has been reported that heterogeneous direct electron transfer between a high potential Laccase (*T. hirsuta*) and gold surface occurs at ca. 0.4 V (vs. NHE). This process was attributed to type 2 Cu site, which was found to be similar for either low or high-potential Laccase, and should be a complex mechanism involving the entire trinuclear T2–T3 copper centers [59]. Thus, it is conceivable to assign the less positive redox process detected in cyclic voltammograms of figure 9 to this electrochemical conversion. The second electrochemical process, more positive, with $E_{1/2}$ ~ 0.47 V, is assigned to the presence of Fe_3O_4 NPs, as deduced from figure S3, in Supplementary Material, and discussed above (section 3.2.1).

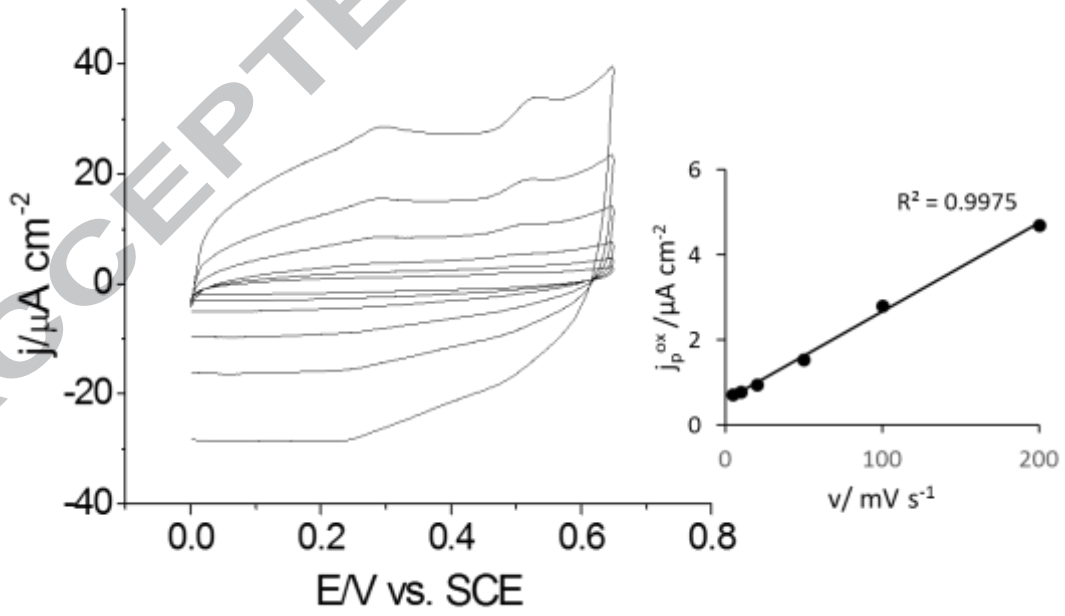

Figure 9 – Cyclic voltammograms of modified electrodes with CS_2/Fe_3O_4 NPs (40 nm)/Laccase in deaerated citrate-phosphate solution (pH 4.6), recorded from 5 to 200 mV s^{-1}. Inset: representation of j_p^{ox} *vs.* υ (upon subtracting the capacitive currents) for the oxidation occurring at ca 0.26 V.

The linear dependence of j_p^{ox} *vs.* υ exhibited in the inset of figure 9 indicates that: i) the electronic transfer is a charge-controlled process (slope of log j_p *vs.* log υ is 0.84), expected for immobilized electroactive species; ii) Fe_3O_4/Laccase nanoconjugates on gold surfaces are stable. The surface concentration of Laccase on modified surfaces with CS_2 and Fe_3O_4 NPs (40 nm) was estimated based on the integration of the oxidation process (figure 9, at 100 mVs^{-1}), by subtracting the capacitive current and considering the transfer of one electron during the direct electrochemical conversion of a Cu catalytic centre of Laccase. A coverage of 2×10^{-11} mol cm^{-2} was obtained, which is a higher value than that estimated for a monolayer coverage of Laccase (4.3×10^{-12} mol cm^{-2}) [58] and for Laccase covalently immobilized on a self-assembled monolayer [60], but analogous to that obtained for Laccase adsorbed onto nanoporous gold supported by a glassy carbon electrode [58].

4. Conclusion

We have developed a novel one-step method to self-assemble (bio)functionalized magnetite nanostructures onto gold electrodes, through the reaction between CS_2, Fe_3O_4 NPs and amine groups of an electroactive compound (epinephrine) or an enzyme (Laccase). This strategy eliminates a number of usual steps involved in surface modification with nanostructures [12,13] and avoids the use of core-shell nanoparticles, such as SiO_2@Fe_3O_4 [30] or Au@Fe_3O_4 [61]. S2p and N1s XPS data unequivocally confirmed the formation of DTC on the gold surface. The presence of Fe_3O_4 NPs on the electrode surface resulted in a higher amount of adsorbed epinephrine with a more facilitated electrochemical conversion of the hydroquinone/quinone forms (negative shift of the redox potential), when compared to the modified electrodes prepared in the absence of iron oxide nanoparticles. This behavior was more pronounced for the larger and less oxidized magnetite nanoparticles (40 nm), highlighting that the degree of oxidation of magnetite-type nanoparticles is a key factor when constructing electrochemical biosensors using these metal oxide nanostructures. The catalytic performance of the modified electrodes with Laccase/magnetite nanoparticles was demonstrated for ABTS oxidation, with a sensitivity of 100 mA M^{-1} cm^{-2}, which is a

comparable or greater value than others reported for Laccase-based biosensors for ABTS [33,57]. In addition, it was also possible to detect the direct electron transfer between the enzyme copper centers and the electrode surface, thus enhancing its applicability in biosensing field. The good electronic communication between enzyme nanoconjugates and the electrode surface should be related with the short, yet robust, linkage provided by the CS_2 molecule. This method is versatile, can be extended for other metallic surfaces and target (bio)molecules and therefore has a huge potential to be applied in any field of interface science that requires surface functionalization.

Notes

The authors declare no competing financial interest.

Acknowledgements

The authors acknowledge Doctor Jorge Correia for the helpful discussions and Doctor Carlos P. M. de Sá for the fruitful support with XPS experiments. This work was funded by Fundação para a Ciência e a Tecnologia: PhD scholarship (SFRH/BD/70673/2010) and projects: PEst 2015-2020-UID/Multi/00612/2013, IF/00808/2013 (POPH, UE-FSE), PTDC/CTM-NAN/0994/2014 and partially by PTDC/CTM-BIO/2102/2012.

References

1. S. C. Barton, H.-H. Kim, G. Binyamin, Y. Zhang and A. Heller, *Journal of the American Chemical Society*, 2001, **123**, 5802-5803.
2. A. Heller, *Physical Chemistry Chemical Physics*, 2004, **6**, 209-216.
3. J. Fei, H.-K. Song and G. T. R. Palmore, *Chemistry of Materials*, 2007, **19**, 1565-1570.
4. C. X. Guo, Z. M. Sheng, Y. Q. Shen, Z. L. Dong and C. M. Li, *ACS Applied Materials & Interfaces*, 2010, **2**, 2481-2484.
5. T. Shimomura, T. Itoh, T. Sumiya, T.-a. Hanaoka, F. Mizukami and M. Ono, *Sensors and Actuators B: Chemical*, 2011, **153**, 361-368.
6. C.-J. Cai, M.-W. Xu, S.-J. Bao, C. Lei and D.-Z. Jia, *RSC Advances*, 2012, **2**, 8172-8178.
7. L. Yang, X. Ren, F. Tang and L. Zhang, *Biosensors and Bioelectronics*, 2009, **25**, 889-895.
8. E. Katz, I. Willner and J. Wang, *Electroanalysis*, 2004, **16**, 19-44.
9. L. M. Rossi, A. D. Quach and Z. Rosenzweig, *Analytical and Bioanalytical Chemistry*, 2004, **380**, 606-613.

10. S.-M. Chen, J.-Y. Chen and V. S. Vasantha, *Electrochimica Acta*, 2006, **52**, 455-465.
11. X. Huang, X. Meng, F. Tang, L. Li, D. Chen, H. Liu, Y. Zhang and J. Ren, *Nanotechnology*, 2008, **19**.
12. J. Hu, B. Yuan, Y. Zhang and M. Guo, *RSC Advances*, 2015, **5**, 99439-99447.
13. Y. Li, C. Qin, C. Chen, Y. Fu, M. Ma and Q. Xie, *Sensors and Actuators B: Chemical*, 2012, **168**, 46-53.
14. M. Martin, P. Salazar, R. Villalonga, S. Campuzano, J. M. Pingarron and J. L. Gonzalez-Mora, *Journal of Materials Chemistry B*, 2014, **2**, 739-746.
15. R. M. C. U. Schwertmann, *The Iron Oxides: Structure, Properties, Reactions, Occurrences and Uses*, Wiley-VCH edn., 2003.
16. S.-L. Tie, Y.-Q. Lin, H.-C. Lee, Y.-S. Bae and C.-H. Lee, *Colloids and Surfaces A: Physicochemical and Engineering Aspects*, 2006, **273**, 75-83.
17. R. Y. Hong, T. T. Pan and H. Z. Li, *Journal of Magnetism and Magnetic Materials*, 2006, **303**, 60-68.
18. A. Goodarzi, Y. Sahoo, M. T. Swihart and P. N. Prasad, in *Quantum Dots, Nanoparticles and Nanowires*, eds. P. GuyotSionnest, H. Mattoussi and Z. L. Wang, 2004, vol. 789, pp. 129-134.
19. D. K. Kim, M. Mikhaylova, Y. Zhang and M. Muhammed, *Chemistry of Materials*, 2003, **15**, 1617-1627.
20. C. Tudisco, F. Bertani, M. T. Cambria, F. Sinatra, E. Fantechi, C. Innocenti, C. Sangregorio, E. Dalcanale and G. G. Condorelli, *Nanoscale*, 2013, **5**, 11438-11446.
21. I. Almeida, A. C. Cascalheira and A. S. Viana, *Electrochimica Acta*, 2010, **55**, 8686-8695.
22. H. Zhu, D. M. Coleman, C. J. Dehen, I. M. Geisler, D. Zemlyanov, J. Chmielewski, G. J. Simpson and A. Wei, *Langmuir*, 2008, **24**, 8660-8666
23. Z.-H. Wang, A. S. Viana, G. Jin and L. M. Abrantes, *Bioelectrochemistry*, 2006, **69**, 180-186.
24. J. A. Rodriguez and J. Hrbek, *Accounts of Chemical Research*, 1999, **32**, 719-728.
25. M. Iwamoto, T. Abe and Y. Tachibana, *Journal of Molecular Catalysis A: Chemical*, 2000, **155**, 143-153.
26. H. Cohen, A. Gedanken and Z. Zhong, *The Journal of Physical Chemistry C*, 2008, **112**, 15429-15438.
27. I. Almeida, S. G. Mendo, M. D. Carvalho, J. P. Correia and A. S. Viana, *Electrochimica Acta*, 2016, **188**, 1-12.
28. R. Rawal, S. Chawla, Devender and C. S. Pundir, *Enzyme and Microbial Technology*, 2012, **51**, 179-185.
29. D. Cao and N. Hu, *Biophysical Chemistry*, 2006, **121**, 209-217.
30. Y. Zhang, G.-M. Zeng, L. Tang, D.-L. Huang, X.-Y. Jiang and Y.-N. Chen, *Biosensors and Bioelectronics*, 2007, **22**, 2121-2126.
31. X. Shi, W. Gu, B. Li, N. Chen, K. Zhao and Y. Xian, *Microchimica Acta*, 2014, **181**, 1-22.
32. L. Tang, G. Zeng, J. Liu, X. Xu, Y. Zhang, G. Shen, Y. Li and C. Liu, *Analytical and Bioanalytical Chemistry*, 2008, **391**, 679-685.
33. D. Quan, Y. Kim and W. Shin, *Journal of Electroanalytical Chemistry*, 2004, **561**, 181-189.
34. K. Piontek, M. Antorini and T. Choinowski, *Journal of Biological Chemistry*, 2002, **277**, 37663-37669.

35. I. Almeida, V. C. Ferreira, M. F. Montemor, L. M. Abrantes and A. S. Viana, *Electrochimica Acta*, 2012, **83**, 311-320.
36. M. Fernández-Fernández, M. Á. Sanromán, D. Moldes, *Biotechnology Advances*, 2013, **31**, 1808–1825.
37. C. Bach, D. Warnock, D. Van Horn, M. Weintraub, R. Sinsabaugh, S. Allison, D. German, *Soil Biology & Biochemistry*, 2013, **67**, 183-191.
38. M. D. Carvalho, F. Henriques, L. P. Ferreira, M. Godinho and M. M. Cruz, *Journal of Solid State Chemistry*, 2013, **201**, 144-152.
39. Y. Niu, A. I. Matos, L. M. Abrantes, A. S. Viana and G. Jin, *Langmuir*, 2012, **28**, 17718-17725.
40. Kai Chen and Hans D. Robinson, *Journal of Nanoparticle Research*, 2011, **13**:751–761.
41. S.-I. Pyun, H.-C. Shin, J.-W. Lee, J.-Y Go, *Electrochemistry of Insertion Materials for Hydrogen and Lithium, Monographs in Electrochemistry*, Springer-Verlag, Berlin Heidelberg, 2012.
42. L. Zhu, R. Zhao, K. Wang, H. Xiang, Z. Shang, W. Sun, *Sensors*, 2008, **8**, 5649-5660.
43. P. Encinas, L. Lorenzo, M. L. Tascon, M. D. Vazquez and P. Sanchezbatanero, *Journal of Electroanalytical Chemistry*, 1994, **371**, 161-166.
44. C. Battocchio, F. Porcaro, S. Mukherjee, E. Magnano, S. Nappini, I. Fratoddi, M. Quintiliani, M. V. Russo, G. Polzonetti, *Journal of Physical Chemistry C*, 2014, **118**, 8159-8168.
45. P. Morf, F. Raimondi, H.-G. Nothofer, B. Schnyder, A.Yasuda, J. M. Wessels, T. A. Jung, *Langmuir*, 2006, **22**, 658-663.
46. D. G. Castner, *Langmuir*, 1996, **12,** 5083-5086.
47. M-C. Bourg, A. Badia, R. B. Lennox, *Journal of Physical Chemistry B*, 2000, **104**, 6562-6567.
48. D. Susac, L. Zhu, M. Teo, A. Sode, K. C. Wong, P. C. Wong, R. R. Parsons, D. Bizzotto, K. A. R. Mitchell, S. A. Campbell, *Journal of Physical Chemistry C*, 2007, **111**, 18715-18723.
49. T. Laiho, J.A. Leiro, J. Lukkari, *Applied Surface Science*, 2003, **212–213,** 525–529.
50. C. Yan, M. Zharnikov, A. Gölzhäuser, M. Grunze, *Langmuir*, 2000, **16**, 6208-6215.
51. N. Graf, E. Yegen, T. Gross, A. Lippitz, W. Weigel, S. Krakert, A.Terfort, W. E.S. Unger, *Surface Science*, 2009, **603**, 2849–2860.
52. S.M. D. Watson, H. D. A. Mohamed, B. R. Horrocksa, Andrew Houlton, *Nanoscale*, 2013, **5**, 5349–5359.
53. D. M. Fernandes, M. Costa. C. Pereira, B. Bachiller-Baeza, I. Rodríguez-Ramos, A. Guerrero-Ruiz, C. Freire, *Journal of Colloid and Interface Science*, 2014, **432,** 207–213.
54. K. Saal, V. Sammelselg, A. Lõhmus, E. Kuusk, G. Raidaru, T. Rinken and A. Rinken, *Biomolecular Engineering*, 2002, **19**, 195-199.
55. I. Zawisza, J. Rogalski and M. Opallo, *Journal of Electroanalytical Chemistry*, 2006, **588**, 244-252.
56. R.S. Nicholson, I. Shain, *Analytical Chemistry*, 1964, **36,** 706-723.
57. A. Jarosz-Wilkołazka, T. Ruzgas and L. Gorton, *Talanta*, 2005, **66**, 1219-1224.
58. H. Qiu, C. Xu, X. Huang, Y. Ding, Y. Qu and P. Gao, *Journal of Physical Chemistry C*, 2008, **112**, 14781-14785.

59. S. Shleev, A. Christenson, V. Serezhenkov, D. Burbaev, A. Yaropolov, L. Gorton and T. Ruzgas, *Biochemical Journal*, 2005, **385**, 745-754.
60. J. F. Cabrita, L. M. Abrantes and A. S. Viana, *Electrochimica Acta*, 2005, **50**, 2117-2124.
61. C.-M. Yu, J.-W. Guo, H.-Y. Gu, *Microchimica Acta*, 2009, **166**, 215–220.

Supplementary Material

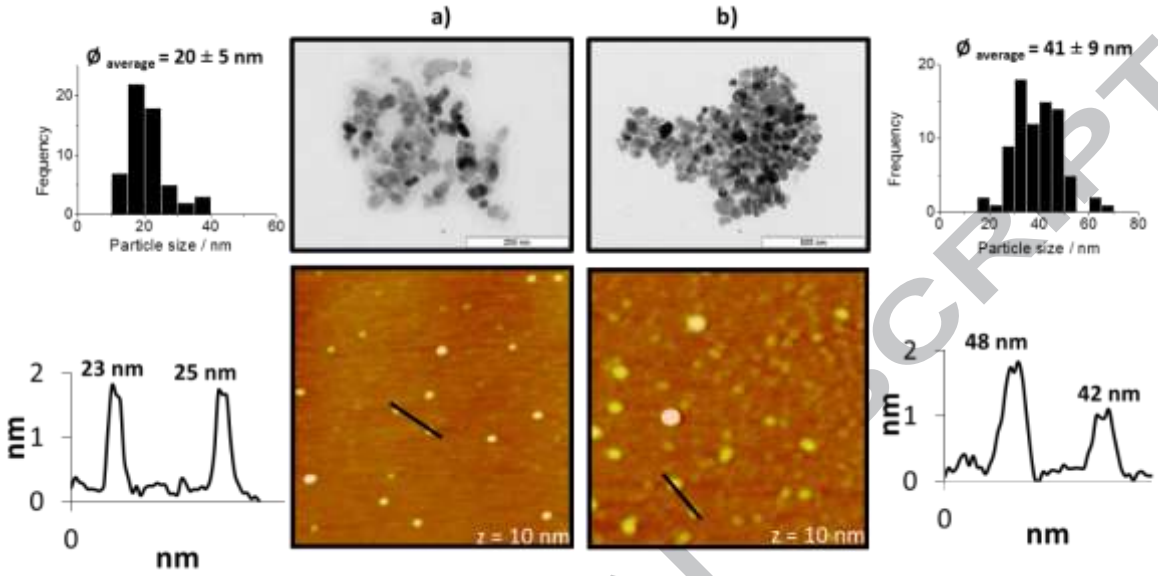

Figure S1 - Images of Fe_3O_4 NPs prepared in a autoclave at 200 ºC for 3 h (a) and 24 h (b). Top row: TEM images and corresponding histograms; bottom row: AFM images (1.0 ×1.0 μm^2; z = 10 nm) of mica after drop casting the aqueous suspension of Fe_3O_4 NPs and corresponding cross sections.

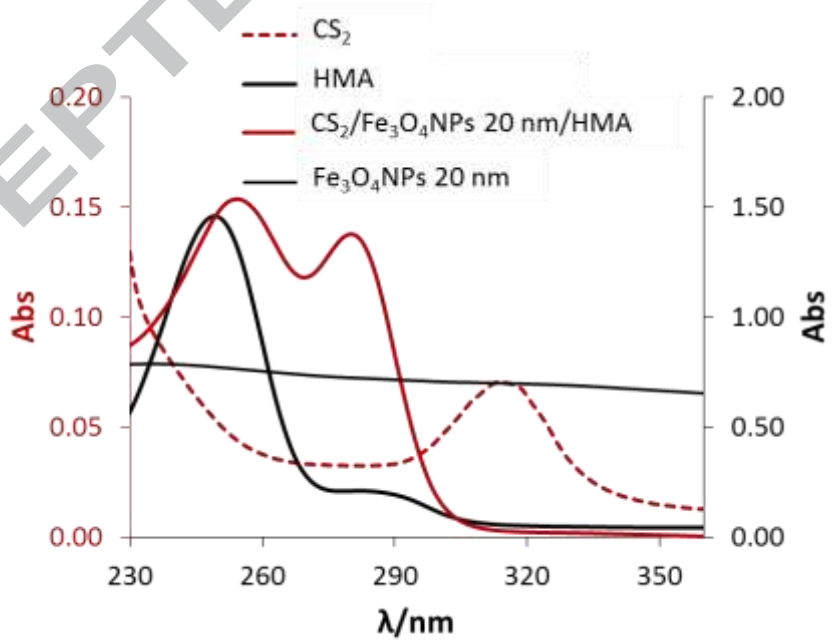

Figure S2 - UV–vis spectra of CS_2, HMA, Fe_3O_4 NPs (20 nm) and CS_2/Fe_3O_4 NPs (20 nm) /HMA, in phosphate buffer solution (concentrations are 0.25 mM and 0.50 mM for CS_2 and HMA, respectively).

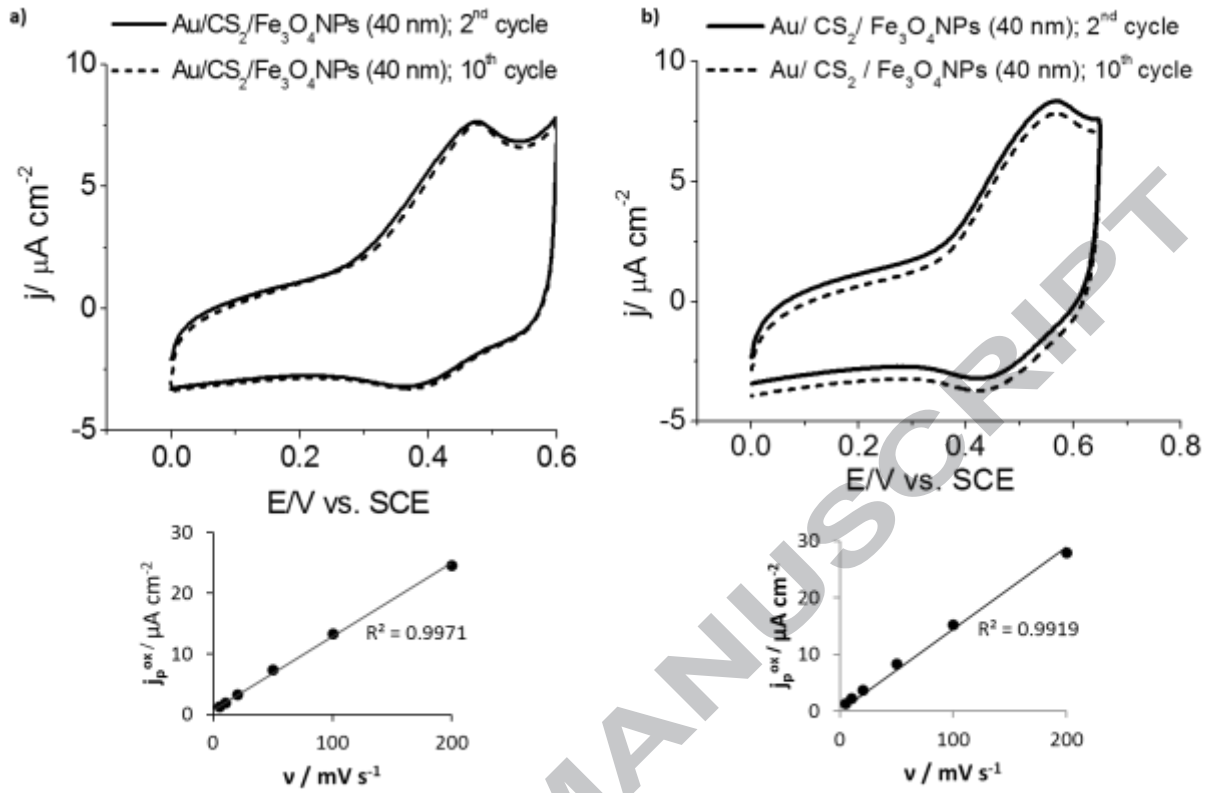

Figure S3 – Cyclic voltammograms (2nd and 10th cycles) of modified gold electrodes with CS_2/Fe_3O_4NPs (40 nm), in a) phosphate buffer solution (pH 7.0) and b) citrate-phosphate buffer solution (pH 4.6) at 50 mV s^{-1}. Inset of figure: j_p^{ox} *vs.* υ.

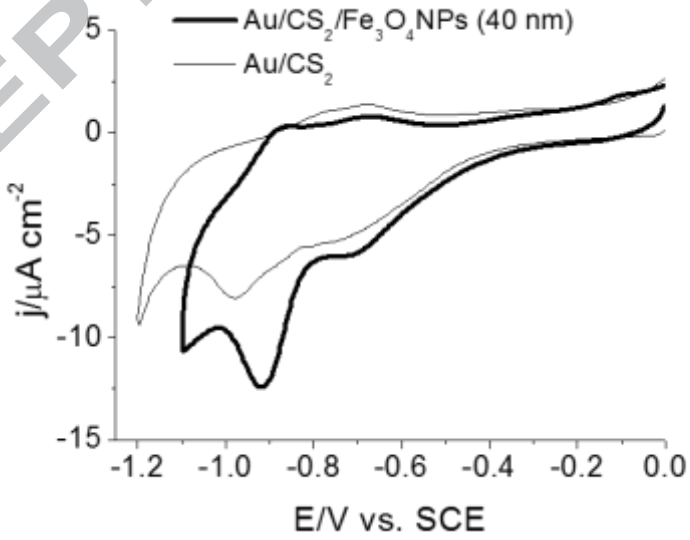

Figure S4- Cyclic voltammograms of modified gold with CS_2 and CS_2/Fe_3O_4 NPs (40 nm) in 0.1 M NaOH, at 20 mV s^{-1}.

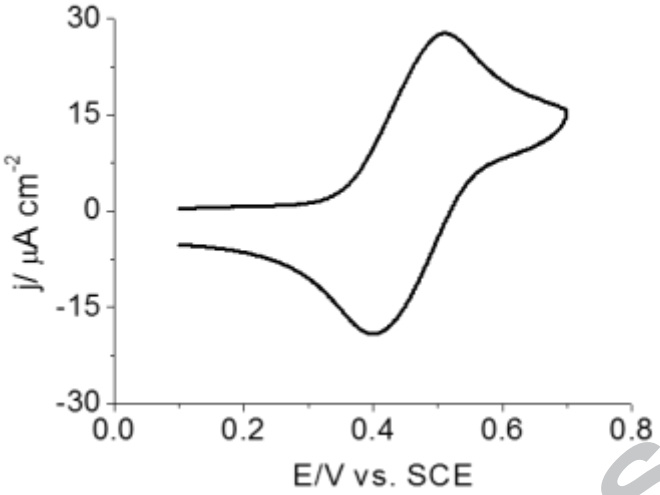

Figure S5 – Cyclic voltammogram of bare gold with 0.5 mM of ABTS in citrate-phosphate buffer solution (pH 4.6), at 20 mV s^{-1}.

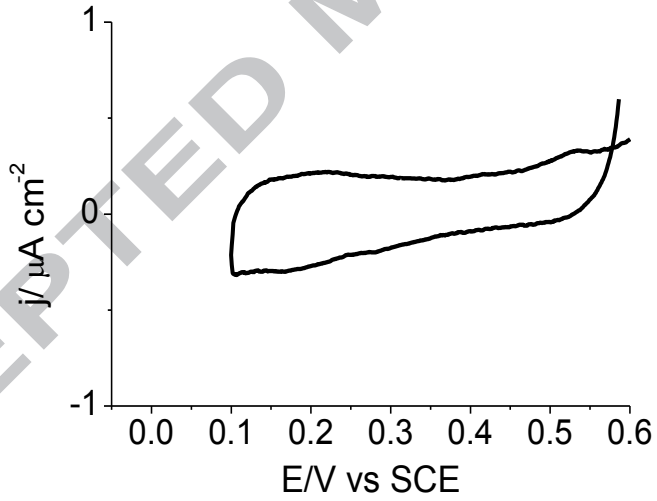

Figure S6 – Cyclic voltammograms recorded at 5 mV s^{-1} in citrate-phosphate solution (pH 4.6) of modified electrode with Laccase/Fe_3O_4 NPs (40 nm) in the presence of 10 μM of ABTS.

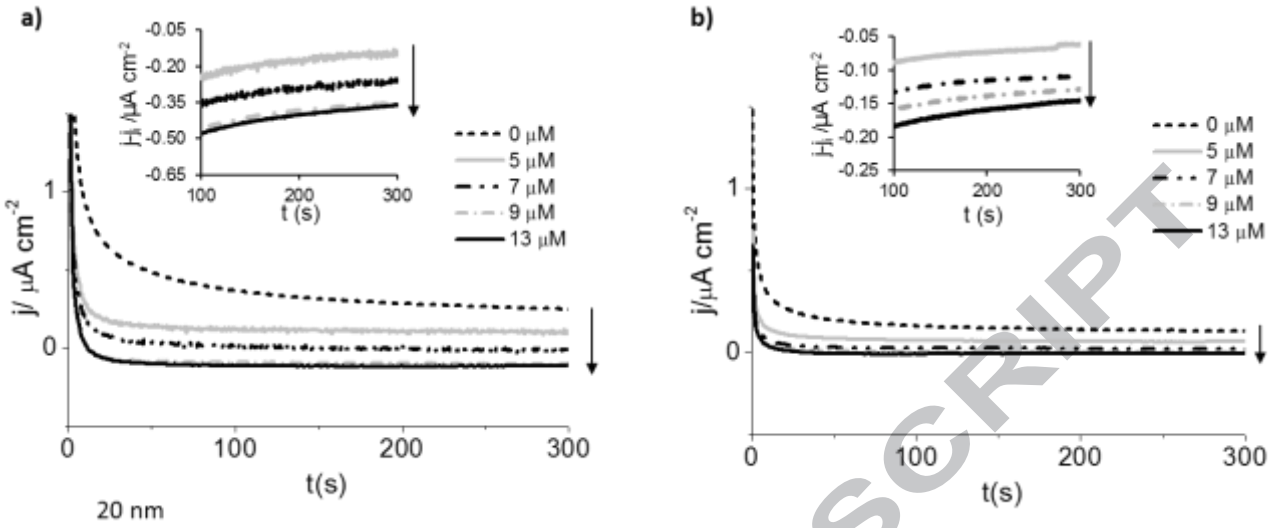

Figure S7 - Chronoamperograms of modified electrodes with a) CS_2/Fe_3O_4 NPs (20 nm)/Laccase and b) CS_2/Laccase obtained for increasing concentrations of ABTS at 0.41 V. Inset of figures: $j-j_i$ *vs.* t

Graphical abstract